A Simple Phenomenological Model for Magnetic Shape Memory Actuators

Johannes Ziske[1], Fabian Ehle[1], Holger Neubert[1], Aaron D. Price[2], and Jens Lienig[1]

[1]Institute of Electromechanical and Electronic Design, Dresden University of Technology, Dresden 01062, Germany
[2]ABB Corporate Research Center Germany, Ladenburg 68526, Germany

This paper presents a new phenomenological model for magnetic shape memory (MSM) alloy actuators. The model was implemented as a lumped element for multi-domain network models using the Modelica language. These network models are rapidly computed and are therefore well suited for MSM-based actuator design and optimization. The proposed MSM model accounts for the 2-D hysteresis of the magnetic field-induced strain as a function of both the applied magnetic flux density and the compressive stress. An extended Tellinen hysteresis formulation was utilized to compute the mechanical strain of the MSM material from measured upper and lower limiting hysteresis surfaces. Two alternative approaches for the computation of the lumped element have been implemented. The first method uses hyperbolic shape functions to approximate the limiting hysteresis surfaces and offers a good balance of simulation accuracy, numerical stability, computational speed, and ease of parameter identification. The second method uses 2-D lookup tables for direct interpolation of the measured limiting hysteresis surfaces, which leads to higher accuracy. Finally, a test case having simultaneously varying compressive stress and magnetic flux density was utilized to experimentally validate both methods. Sufficient agreement between the simulated and measured strain of the sample was observed.

Index Terms—**Hysteresis, lumped network model, magnetic shape memory (MSM) alloy, multi-domain.**

I. INTRODUCTION

MAGNETIC shape memory (MSM) alloys are smart materials, which exhibit large field-induced strain (typically ~6%) when exposed to a magnetic field of sufficient strength. MSM materials have been under investigation as a new class of active material actuators since the middle of the 1990s [1], [2]. The development, availability, and quality of these materials has dramatically improved since the time of these early studies.

Despite these advances, very few prototypes for the industrial application of MSM-based actuators have been reported [3], [4]. This dearth is partly due to the highly nonlinear and complex magnetomechanical properties of the material, which complicates MSM actuator design and optimization. In this regard, fast computing and easy-to-use representations are desirable for use in multi-domain network models. These types of models are state-of-the-art for the design of conventional actuator systems (e.g. electromagnetic actuators [5], [6]), and couple multiple physical domains, including electronic circuits, control units, and mechanical loads. Network models are typically implemented in object-oriented description languages like Modelica or VHDL-AMS to support reusability.

In order to establish a network modeling approach for MSM actuators, models are required which: 1) represent the material behavior accurately enough for actuator design; 2) enable straightforward parameter fitting to measurements; and 3) can be readily integrated into multi-domain network models. In the context of actuator design, the physical interpretation of the model parameters and spatial distribution of the magnetic field, strain, and stress in the interior of the MSM alloy are of secondary importance. Therefore, spatially concentrated 1-D models are typically sufficient.

Several models of the 3-D hysteresis of the strain $\varepsilon(B, \sigma)$ of MSM alloys as a function of the mechanical stress σ and strain ε along the load axis, and orthogonal magnetic flux density B have been proposed. These models are typically classified according to either a microscopic or macroscopic approach [4]. Microscopic approaches primarily address the properties and physics of these alloys and are intended to enhance the fundamental understanding of the material [7], [8].

In contrast, macroscopic approaches are more appropriate for system design. Sectionwise linear approximation of the MSM hysteresis is described in [9] and [10]. This approach results in significant deviations at the beginning and the end of the twin boundary movement. Moreover, the non-differentiability at the switchover points between the separate approximation sections introduces numerical instabilities.

In an effort to improve the open- and closed-loop control of MSM-based actuators, modified Preisach and Prandtl–Ishlinsky hysteresis models have been applied in [11] and [12]. The temperature dependence of the hysteresis is accounted for by multiple parameter sets and interpolation between them. However, this approach only captures hysteresis of strain as a function of the applied currents. Mechanical components of the actuator system (such as the bias spring) are incorporated within these parameter sets. Therefore, non linear or time-dependent mechanical loads cannot be considered.

In [13]–[15], the Preisach model was extended to two inputs to model the strain hysteresis of magnetostrictive materials and has been utilized for compensation and control of two-input hysteresis systems. The results are promising, but the complex implementation of the dual-input Preisach model as well as the laborious parameterization, for which a large number of first-order reversal curve measurements and their analysis is needed, restricts the application potential for the desired task.

Manuscript received March 2, 2014; revised May 23, 2014; accepted July 7, 2014. Date of publication July 11, 2014; date of current version January 26, 2015. Corresponding author: J. Ziske (e-mail: johannes.ziske@tu-dresden.de).

Color versions of one or more of the figures in this paper are available online at http://ieeexplore.ieee.org.

Digital Object Identifier 10.1109/TMAG.2014.2338833

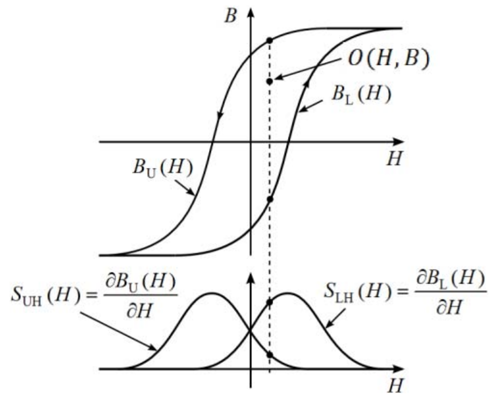

Fig. 1. Upper $B_U(H)$ and lower $B_L(H)$ branches of the hysteresis envelope curve, with corresponding slope functions $S_{UH}(H)$ and $S_{LH}(H)$ about an operating point O.

A purely phenomenological hysteresis model has been reported in [16]. Exponential functions represent the $\varepsilon(B)$ hysteresis, however, hysteresis due to mechanical loading effects is not considered. This approach formed the basis of a dynamic simulation and design optimization of an MSM-based tripping unit for low-voltage switch gear. Drawbacks inherent to the reported approach were attributed to neglecting the mechanical hysteresis, resulting in inaccuracies for inner hysteresis loops under partial strain. The approach is also computationally expensive for non-constant loads (typical operating conditions) since the approximation functions of the hysteresis behavior must be recomputed in every time step.

In summary, no sufficient models for MSM elements are known to exist that are capable of supporting the design of MSM actuators using a network model approach. In this investigation, we introduce a solution based on an extended Tellinen hysteresis model (Section II), which is subsequently implemented in Modelica and validated for an Adaptamat MSM sample (Section IV). The experimental setup, methods, and results are described in Section III.

II. Modeling Approach

A. Tellinen Hysteresis Model

The Tellinen hysteresis model was first introduced as a simple phenomenological description of ferromagnetic hysteresis behavior [17]. It enables the computation of arbitrary hysteresis curves, including outer and inner loops based only on the hysteresis envelope curve. The model is completely configured with the upper $B_U(H)$ and lower $B_L(H)$ branch of the limiting hysteresis loop of a certain ferromagnetic material (Fig. 1). The corresponding slope functions $S_{UH}(H)$ and $S_{LH}(H)$ can directly be derived from $B_U(H)$ and $B_L(H)$

$$S_{UH}(H) = \frac{\partial B_U(H)}{\partial H}, \quad S_{LH}(H) = \frac{\partial B_L(H)}{\partial H}. \tag{1}$$

The Tellinen model requires

$$\frac{dB}{dt} = k_H\left(B, \frac{dH}{dt}\right) \cdot \frac{dH}{dt} \tag{2}$$

to be fulfilled at any time during transient simulation of a magnetic material with hysteresis. Equation (2) defines

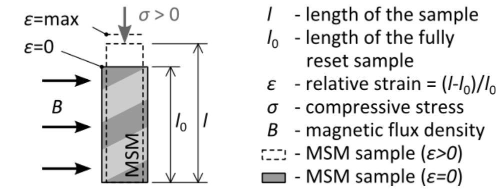

Fig. 2. Typical arrangement of the MSM sample and used quantities.

$k_H(B, dH/dt)$ as the ratio between the slope dB/dt and the time derivative dH/dt of the magnetic field strength at the operating point $O(H,\ B)$. A linear scaling of the slope function by the instantaneous position of the operating point $O(H,\ B)$ is assumed at any operating point within the hysteresis envelope. The factor k_H is separately defined for rising and falling magnetic field strengths

$$k_H = \begin{cases} \dfrac{B_U(H) - B}{B_U(H) - B_L(H)} \cdot S_{LH}(H) & \text{for } \frac{dH}{dt} > 0 \\ \dfrac{B - B_L(H)}{B_U(H) - B_L(H)} \cdot S_{UH}(H) & \text{for } \frac{dH}{dt} < 0. \end{cases} \tag{3}$$

B. Extension of Tellinen Model to Two Dimensions

The model presented here is purely phenomenological and based on measurement data. It describes the scalar and quasi-static field-induced uniaxial strain of a MSM sample according to the typical arrangement of a MSM element within an actuator as shown in Fig. 2. It assumes a uniform magnetic flux density through the sample perpendicular to the axis of strain and stress. In addition, in accordance with the typical arrangement, only compressive stresses ($\sigma \geq 0$) are supported, although the model would be capable of considering tensile stresses as well. The relative strain is related to the length of the fully reset and tension-free sample.

The standard Tellinen model describes the hysteresis behavior of B with regard to a single input H. To adequately model the mechanical strain ε of an MSM element in electromagnetomechanical system models, at least two inputs must be considered: the magnetic flux density B through the sample and the applied compressive stress σ.

Thus, the limiting hysteresis curves of the Tellinen model develop to limiting hysteresis surfaces of ε over the B-σ plane.

Since MSM samples respond with the same strain under positive and negative flux densities (limiting hysteresis surfaces are symmetric mirrored at the ε-σ plane), it is sufficient to describe the surfaces only for $B \geq 0$ and to use $B* = |B|$ as the model input. Fig. 3(a) shows exemplarily the upper and lower limiting hysteresis surfaces $\varepsilon_U(B^*,\sigma)$ and $\varepsilon_L(B^*,\sigma)$, respectively. Based on $\varepsilon_U(B^*,\sigma)$ and $\varepsilon_L(B^*,\sigma)$, four slope functions $S_{UB}(B^*,\sigma)$, $S_{LB}(B^*,\sigma)$, $S_{U\sigma}(B^*,\sigma)$, and $S_{L\sigma}(B^*,\sigma)$ can be derived as the partial derivatives

$$S_{UB}(B^*,\sigma) = \frac{\partial \varepsilon_U(B^*,\sigma)}{\partial B^*}, \quad S_{LB}(B^*,\sigma) = \frac{\partial \varepsilon_L(B^*,\sigma)}{\partial B^*} \tag{4}$$

$$S_{U\sigma}(B^*,\sigma) = \frac{\partial \varepsilon_U(B^*,\sigma)}{\partial \sigma}, \text{ and } S_{L\sigma}(B^*,\sigma) = \frac{\partial \varepsilon_L(B^*,\sigma)}{\partial \sigma}. \tag{5}$$

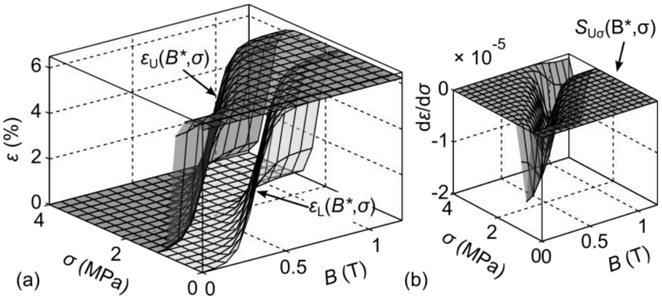

Fig. 3. (a) and (b) Example limiting upper $\varepsilon_{\mathrm{U}}(B^*,\sigma)$ and lower $\varepsilon_{\mathrm{L}}(B^*,\sigma)$ hysteresis surfaces over the B-σ plane and the corresponding slope function $S_{\mathrm{U}\sigma}(B^*,\sigma)$.

A typical $S_{\mathrm{U}\sigma}(B^*,\sigma)$ slope function is shown in Fig. 3(b).

By extending (2), the time derivative of ε is the sum of two terms depending on the time derivatives of B^* and σ, respectively, and using the factors k_{B} and k_σ

$$\frac{d\varepsilon}{dt} = k_{\mathrm{B}}\left(B^*, \sigma, \frac{dB^*}{dt}\right) \cdot \frac{dB^*}{dt} + k_\sigma\left(B^*, \sigma, \frac{d\sigma}{dt}\right) \cdot \frac{d\sigma}{dt}. \quad (6)$$

In analogy to the Tellinen model, k_{B} and k_σ are defined as

$$k_{\mathrm{B}} = \begin{cases} \dfrac{\varepsilon_{\mathrm{U}}(B^*,\sigma) - \varepsilon}{\varepsilon_{\mathrm{U}}(B^*,\sigma) - \varepsilon_{\mathrm{L}}(B,\sigma)} \cdot S_{\mathrm{LB}}(B^*,\sigma) & \text{for } \frac{dB^*}{dt} > 0 \\ \dfrac{\varepsilon - \varepsilon_{\mathrm{L}}(B,\sigma)}{\varepsilon_{\mathrm{U}}(B^*,\sigma) - \varepsilon_{\mathrm{L}}(B,\sigma)} \cdot S_{\mathrm{UB}}(B^*,\sigma) & \text{for } \frac{dB^*}{dt} < 0 \end{cases} \quad (7)$$

and

$$k_\sigma = \begin{cases} \dfrac{\varepsilon - \varepsilon_{\mathrm{L}}(B^*,\sigma)}{\varepsilon_{\mathrm{U}}(B^*,\sigma) - \varepsilon_{\mathrm{L}}(B^*,\sigma)} \cdot S_{\mathrm{U}\sigma}(B^*,\sigma) & \text{for } \frac{d\sigma}{dt} > 0 \\ \dfrac{\varepsilon_{\mathrm{U}}(B,\sigma) - \varepsilon}{\varepsilon_{\mathrm{U}}(B^*,\sigma) - \varepsilon_{\mathrm{L}}(B^*,\sigma)} \cdot S_{\mathrm{L}\sigma}(B^*,\sigma) & \text{for } \frac{d\sigma}{dt} < 0. \end{cases} \quad (8)$$

The model is of quasi-static nature. In (6), ε has only an implicit time dependence from B^* and σ. The slope functions (7) and (8) involve directional derivatives, and only the signs of time derivatives are used to determine the direction of both stress and field change. However, a quasi-static material model covers most typical actuator configurations of MSM alloys in which the change rates of both stress and magnetic field are limited by the inertia of the load and the inductivity of the magnetic excitation circuit, respectively. This also applies to the test case in Section IV-B.

C. Hysteresis Envelope Surface Approximation Using Trial Functions

An analytical description of the $\varepsilon_{\mathrm{L}}(B^*,\sigma)$ and $\varepsilon_{\mathrm{U}}(B^*,\sigma)$ surfaces and their slope functions $S_{\mathrm{UB}}(B^*,\sigma)$, $S_{\mathrm{LB}}(B^*,\sigma)$, $S_{\mathrm{U}\sigma}(B^*,\sigma)$, and $S_{\mathrm{L}\sigma}(B^*,\sigma)$ is advantageous for fast computing and numerically stable lumped network elements. For this reason, simple hyperbolic trial functions have been developed to describe the hysteresis surfaces analytically

$$\begin{aligned} \varepsilon_{\mathrm{L}}(B^*,\sigma) = {} & \frac{1}{4} E \cdot \{1 + \tanh[M_1(\sigma - \sigma_2)]\} \\ & \cdot \left\{1 - \tanh[M_3 B^*(n_1 + M_2\sigma)]\right\} \end{aligned} \quad (9)$$

$$\begin{aligned} \varepsilon_{\mathrm{U}}(B^*,\sigma) = {} & \frac{1}{2} E \cdot \{1 - \tanh[M_1(\sigma - \sigma_2)]\} \\ & \cdot \Bigg(1 - \frac{1}{4} \cdot \left\{1 + \tanh[M_4(\sigma - \sigma_3)]\right\} \\ & \cdot \left\{1 + \tanh[M_3 B^*(n_2 + M_2\sigma)]\right\}\Bigg). \end{aligned} \quad (10)$$

The parameters σ_1 to σ_3, n_1 to n_2, and M_1 to M_4 are shift and slope parameters, respectively, and are used to tune the surfaces in accordance with measured hysteresis characteristics. The symbol E denotes the maximum relative strain ε. The partial derivatives of (9) and (10) are the corresponding analytic slope functions.

Measurements, parameter identification, and plot of the adapted trial functions are provided in Section III for an MSM element manufactured by Adaptamat Ltd. (Finland).

D. Hysteresis Envelope Surfaces Based on Interpolated Measurements

Measurements on MSM samples from different suppliers have revealed that the proposed trial functions are not suitable for providing a single universal material representation with sufficient accuracy. On the contrary, finding and fitting adequate trial functions for each material is a laborious task.

For this reason, an alternative approach was developed, which directly interpolates hysteresis surfaces from measurement data. This method is both elegant and versatile, provided that the necessary measurement data are available in sufficient quality for each material under consideration.

To obtain accurate hysteresis surfaces, the strain behavior of the MSM sample is scanned in sufficient intervals throughout a section of interest in the B-σ plane (Section III). The measured hysteresis surfaces are slightly smoothed and mapped onto an equidistant grid via MATLAB script. Linear interpolation between the grid points is later applied in the model implementation (Section IV-A). This allows a continuous computation of the lower and upper hysteresis surface values at the current operating point. Computing these values for two additional points, which have a small B and σ offset, respectively, permits the determination of the local partial derivatives.

E. Magnetic Characteristics Model

The proposed $\varepsilon(B,\sigma)$ model is independent of magnetic characteristics of the MSM sample. However, since the sample is placed in an air gap of a magnetic circuit, its magnetization considerably influences the magnetic resistance of that circuit, and hence the magnetic system behavior. Thus, for the practical use of the $\varepsilon(B,\sigma)$ model, the magnetic characteristics of the MSM sample needs to be considered as well.

The magnetization of the MSM sample depends on both, the applied magnetic field strength H and strain ε of the sample [18]. We derived a magnetic characteristics model

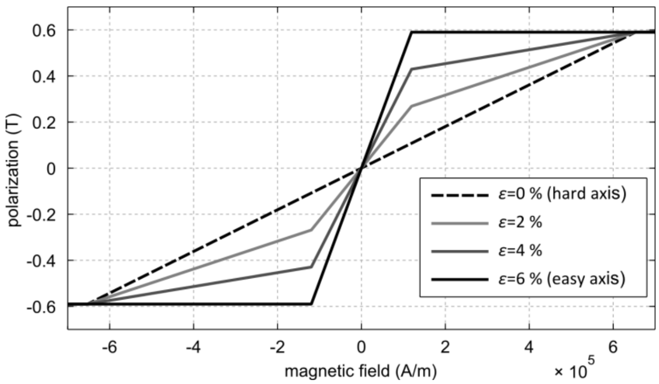

Fig. 4. Implemented simplified model of the H- and ε-dependent magnetic polarization of the MSM sample.

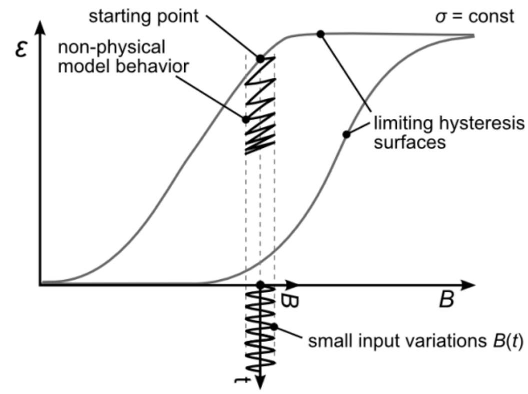

Fig. 5. Non-physical model behavior starting near the limiting hysteresis surface due to small input variations.

from published magnetization curves of NiMnGa [18], [19]. It is assumed that the magnetic easy and hard axis correspond to a fully extended ($\varepsilon = 6\%$) and compressed sample ($\varepsilon = 0\%$), respectively. The magnetization curves can be linearized in a good approximation. Furthermore, a linear relationship between the samples strain and slope of the magnetization curves is assumed as shown in Fig. 4. With respect to the saturation field strength, the material shows only weak hysteresis [19, Fig. 3]. This has only slight influence on system behavior in potential actuator applications and is therefore neglected.

F. Model Limitations

In addition to the model limitations described in Section II-B (stress and strain axis in parallel, magnetic flux axis perpendicular, compressive stresses only), the Tellinen hysteresis model is also subject to some limitations. Due to the lack of a real memory of the quasi-static Tellinen hysteresis model, ε is solely determined by the hysteresis envelope surfaces, the actual operating point (B, σ, ε), and the change in B and σ. Thus, this model does not fulfill the congruency or the path independence property, which were specified for the Preisach hysteresis model with two inputs [13].

Under certain conditions, small periodic input variations lead to unphysical model behavior. Exemplarily, Fig. 5 shows the model reaction to a small periodic variation in B. In particular, this behavior occurs if the starting point is located near the hysteresis envelope surface at a point with high slope.

This behavior restricts the application of the proposed model in, e.g. vibration control. Most actuator applications, however, exploit large strokes and remain unaffected from this restriction. In contrast to these limitations, the decisive advantages of the generalized Tellinen model are the easy implementation, and the low effort in material characterization and model parameterization. This is even more important because the available materials show remarkable variance in their characteristics and therefore a large number of samples need to be modeled to validate an actuator design.

III. Experimental Investigations

A. Measurement Setup

The test apparatus is conceptually illustrated in Fig. 6. It is based on the setup presented in [20] with additional improvements to facilitate the accurate characterization of the hysteresis envelope surfaces of MSM samples. The primary components consist of a magnetic circuit for generating the excitation field, a mechanical assembly for load application, control and measurement, and sensors for strain measurement and data acquisition.

The magnetic circuit consists of a laminated iron core with an air gap for the MSM sample and excitation coils driven by a bipolar power amplifier (KEPCO BOP 72-6M). A maximum flux density of 1.5 T is achieved.

The mechanical load assembly consists of a load cell, weak tension spring, and stepper motor-driven linear bearing arranged in series. This arrangement enables automated load control during the measurement, which is necessary for the measurements of the hysteresis envelopes. Applied loads ranging from 0.25–15 N are possible.

A high-precision laser triangulator (Keyence LK-G82) and magnetic Gauss meter (Magnet-Physik FH 55) are used to measure the sample strain and flux density, respectively. Furthermore, a specialized sample holder was designed to minimize friction and inertial effects.

The data acquisition system (Data Translation DT9806) simultaneously captures B, σ, ε, and the current I during the measurement process. The current I and the stress σ can be controlled independently. This facilitates versatile and fully automated measurement sequences.

B. Measurement Methods and Results

The aforementioned measurement setup facilitates the quasi-static characterization of MSM samples. The magnetic characteristics of the MSM sample causes a minor inhomogeneity of the flux density within the air gap and sample. The flux density is slightly increased near the upper and lower end face of the sample. Thus, the flux density measured directly in between the magnetic core and middle of the MSM sample differs from MSM sample's mean flux density. Using the magnetic characteristics of Fig. 4, this difference was estimated by

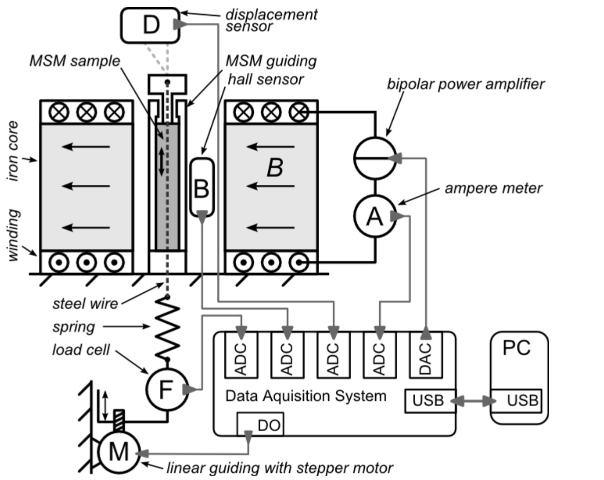

Fig. 6. Measurement setup for MSM sample characterization with low moving mass, low friction guidance, high accuracy load cell, and optical displacement sensor.

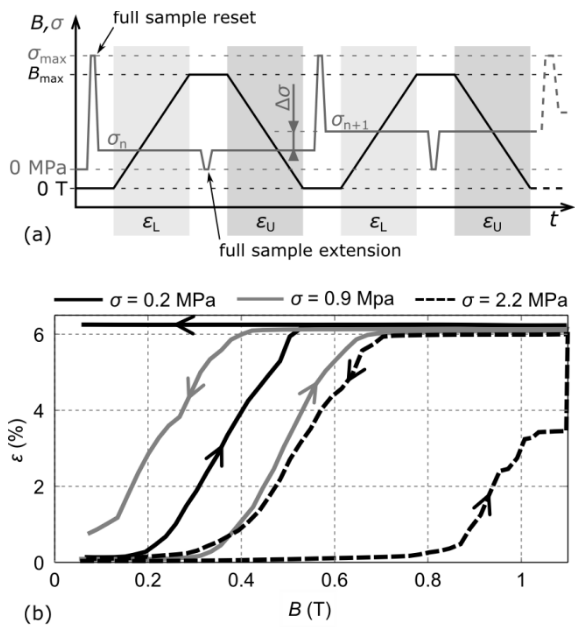

Fig. 7. (a) Method 1 for the measurement of the hysteresis envelope surfaces in B-direction. (b) Measured hysteresis cycles under three different compressive stresses of 0.2, 0.9, and 2.2 MPa.

means of a finite element model of the magnetic circuit. Depending on H and ε, the mean flux density in the sample was found to be 8%–16% higher than in the hall probe. Based on these investigations, the measured flux density can be easily corrected to relate the measurements to the sample's flux density. Nevertheless, the following figures are related to the measured flux density.

Two different measurement methods have been developed for the fully automated scanning of the upper and lower hysteresis envelope surfaces. The methods differ in the manner in which the resulting sample strain ε is scanned over the B-σ plane. Method 1 continuously varies the magnetic flux density B under constant compressive stress σ. In successive cycles, σ is increased by $\Delta\sigma$. In contrast, Method 2 varies

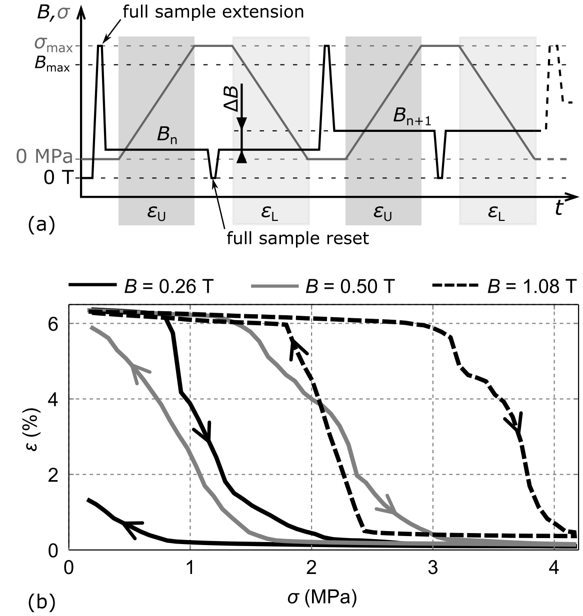

Fig. 8. (a) Method 2 for the measurement of the hysteresis envelope surfaces in σ-direction. (b) Measured hysteresis cycles for three different flux densities of 0.26, 0.50, and 1.08 MPa.

σ continuously at constant B, and B is increased between successive cycles by ΔB.

To effectively measure the hysteresis envelope surfaces (and exclude any inner surfaces), the MSM sample must be completely reset and extended at the beginning and middle of each cycle, respectively. Thus, for Method 1 at the beginning of each B cycle when $B = 0$ T, σ is momentarily set to maximum to ensure a complete reset (i.e., complete strain recovery). During the subsequent increase of B, the observed strain propagates along the lower limiting hysteresis surface ε_L. At maximum B, σ is momentarily reduced to 0 MPa again to allow a full expansion of the sample. During the subsequent reduction of B, a strain curve on the upper limiting hysteresis surface ε_U is observed. Fig. 7 schematically depicts measurement Method 1 and associated cycles under three different loads. These measurements have been conducted using an MSM sample (20 mm × 2 mm × 1.4 mm) manufactured by Adaptamat Ltd. in 2007. The 20 and 1.4 mm directions define the axis of extension and of the magnetic flux, respectively.

In the second method, B is set to maximum at the start of each cycle ($\sigma = 0$ MPa) to assure a full sample extension. The subsequent linear increase of σ corresponds to ε_U. At maximum σ, B is set to 0 T for a short time to fully reset the sample. In the subsequent decrease of σ, the strain of the sample moves along ε_L. Fig. 8 illustrates Method 2 and shows measured hysteresis cycles at three different flux densities.

The apparatus measures the hysteresis envelope surfaces over the B-σ plane in the range of $0 \text{ T} < B < 1.2$ T and $0 \text{ MPa} < \sigma < 4.2$ MPa. Due to the high degree of automation, high repeatability and dense scanning is achievable. The B-σ plane scanning with Method 1 uses a load increment $\Delta\sigma$ of 0.05 MPa, whereas Method 2 used a flux density increment ΔB of 0.02 T. Figs. 9 and 10 show a subset (one quarter) of the

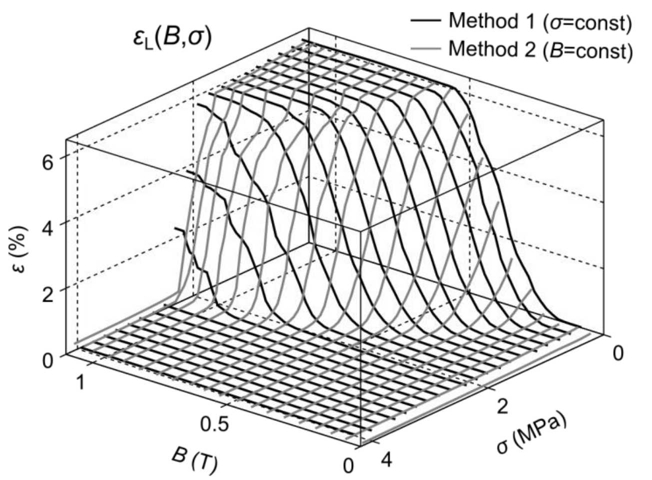

Fig. 9. Measured curves of the lower hysteresis surface $\varepsilon_L(B,\sigma)$ of the Adaptamat MSM sample according to measurement Methods 1 and 2.

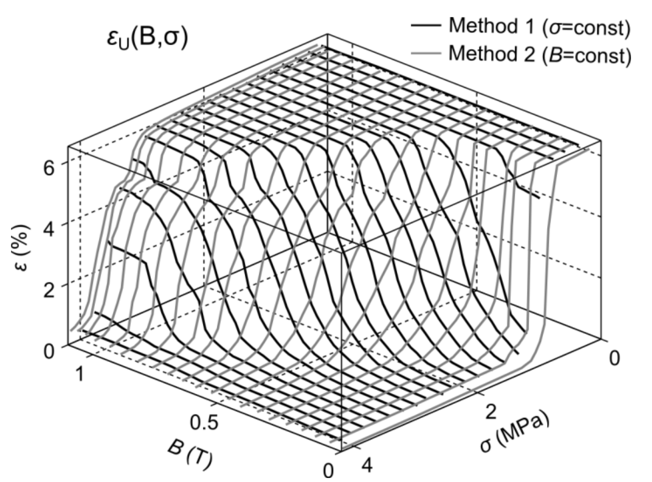

Fig. 10. Measured curves of the upper hysteresis surface $\varepsilon_U(B,\sigma)$ of the Adaptamat MSM sample according to measurement Methods 1 and 2.

measured curves using both methods to determine the lower and upper hysteresis envelope surface, respectively.

As indicated in Figs. 6 and 7, the measurements according to Methods 1 and 2 are in very good agreement for both surfaces. This observation indicates that the proposed modeling approach for the limiting hysteresis surfaces is justified and permissible.

C. Parameter Identification

Based on the measured hysteresis surfaces, the trial functions (9) and (10) presented in Section II-C have been defined. The MATLAB fit-function contained in the curve fitting toolbox was used to fit the functions to the measurement data. As the proposed functions are well-conditioned and not overly complex, parameter identification can also be performed manually. Fig. 11 illustrates the fitted surfaces together with an extraction of the Method 1 measurement data. It can be seen that these functions fit the surfaces of the sample very well. The corresponding identified parameters are listed in Table I.

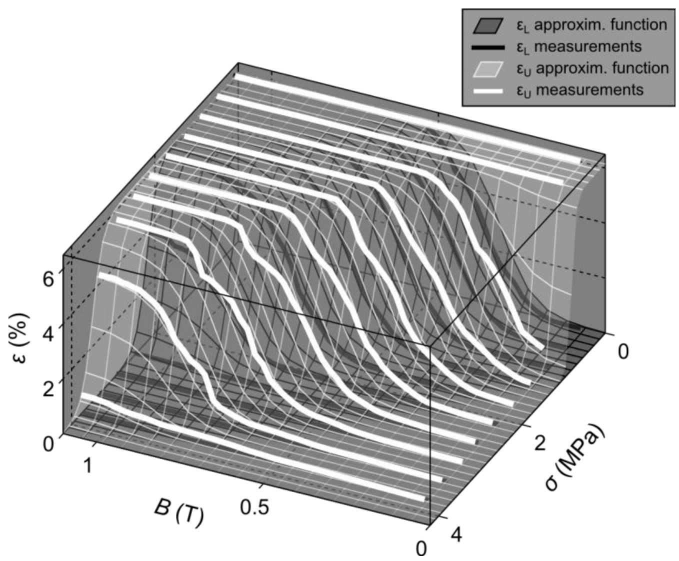

Fig. 11. Measured lower (black lines) and upper (white lines) limiting hysteresis curves and corresponding fitted limiting hysteresis surfaces (thinner grid lines).

TABLE I
IDENTIFIED PARAMETERS OF MSM SAMPLE FROM ADAPTAMAT LTD

Parameter	Value	Unit
E	6.25	%
M_1	4.00e-6	1/Pa
M_2	0.25e-6	1/Pa
M_3	10	1/T
M_4	10e-6	1/Pa
σ_1	2.20e6	Pa
σ_2	3.50e6	Pa
σ_3	0.80e6	Pa
n_1	0.32	-
n_2	0	-

IV. MODEL VALIDATION

A. Model Implementation

The multi-domain modeling language Modelica was used to implement the MSM element model described in Section II. All simulations have been performed in Dymola 2013. The measurement setup provided in Section III has been modeled using the developed MSM element in order to compare simulation and measurement results. Fig. 12 depicts the schematic view of the simulated model. Like the measurement setup, the simulated model consists of a power supply, an excitation winding, a magnetic core, the MSM element, and a bias spring with controllable position. The lumped MSM element has additional connectors to the magnetic domain (air gap) and mechanical domain (mechanical output of the sample). Thus, it can be directly inserted within the magnetic circuit subsystem and connected to the mechanical load subsystem of the network model.

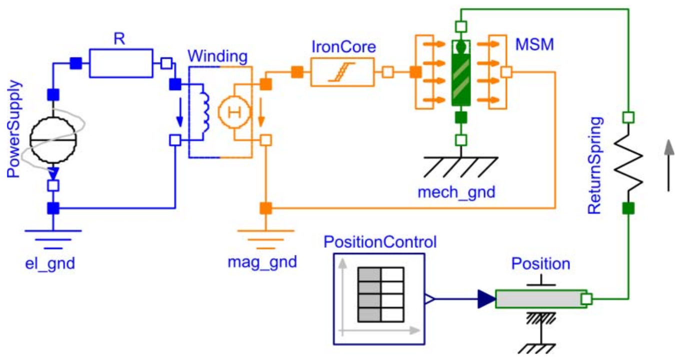

Fig. 12. Modelica multi-domain network model of the measurement setup according to Fig. 6, including the electrical excitation, magnetic circuit, and mechanically loaded MSM sample within the air gap.

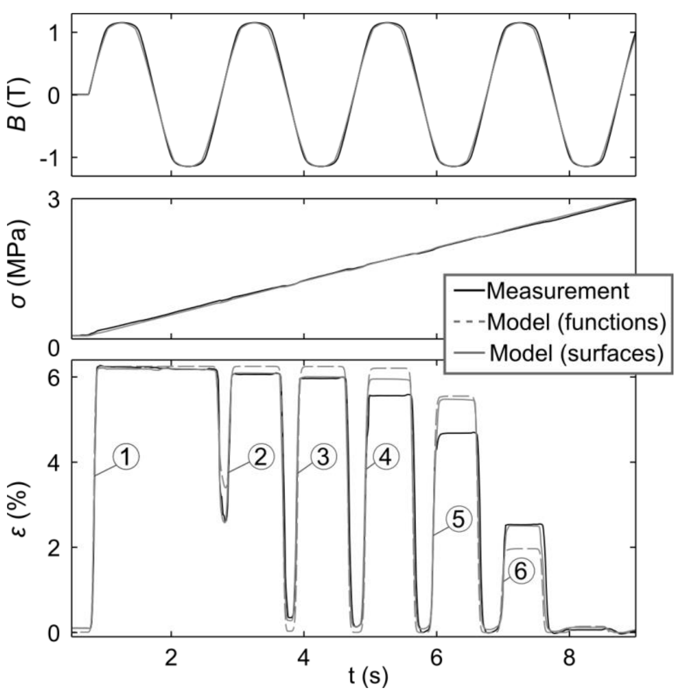

Fig. 13. Comparison of measurements and simulation results of the MSM strain exposed to simultaneously varying flux density and compressive stress.

B. Comparison of Simulation Results to Measurements

A test case was utilized to directly compare simulation results to measurement data. The MSM sample was loaded with simultaneously varying flux density B and compressive stress σ. A sinusoidal current with a frequency of 0.5 Hz is prescribed, which yields a nearly sinusoidal flux density in the air gap with an amplitude of $\sim$1.1 T. In parallel, the spring is linearly elongated resulting in a ramped compressive stress increasing from 0 to 3 MPa.

Dynamic mechanical and electromagnetic effects in the sample, such as inertia and eddy currents, can be neglected in the frequency range applied here. Estimates reveal stress from accelerating forces at least two orders of magnitude lower than static stress. Taking into account the electrical conductivity, maximum permeability and sample dimensions, the cutoff frequency is $>$500 Hz. This is consistent with results from publications, which describe the MSM effect to be quasi-static up to the kilohertz range [21].

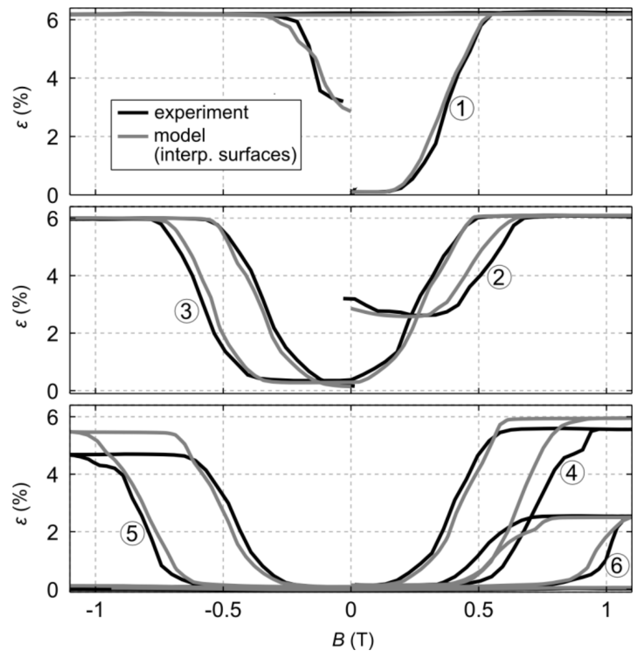

Fig. 14. Butterfly loops of the mechanical strain versus magnetic flux density corresponding to Fig. 13.

Fig. 13 indicates the measurements of B, σ, and ε together with simulation results from both MSM models: 1) one using adapted hyperbolic trial functions and 2) the other using interpolation of measured hysteresis surfaces. Fig. 14 shows the corresponding butterfly loops of the strain ε over the flux density B.

The test case reveals a reasonable agreement between the measurements and simulated model behavior. Higher deviations observed at certain points are attributed to the steep slope of the hysteresis surfaces at these points. In these locations, small variations in measurement conditions between the measurement of the hysteresis surfaces and measurement of the test case can already lead to significant differences. We also note that the measurement conditions are influenced by slightly varying sample positions after assembling, friction, and temperature for which the lumped scalar MSM model does not account for.

The modeling method using interpolated hysteresis surfaces is slightly more accurate than the approach using trial functions. It is anticipated that these differences will be more significant for MSM samples whose hysteresis envelope surfaces cannot be captured as well as those of the example included herein.

In general, the good agreement between the simulated and measured mechanical strain indicates that this extended Tellinen approach can be successfully applied for the phenomenological modeling of the 2-D hysteresis behavior of MSM elements if the mentioned restrictions are taken into account.

V. Conclusion

This paper described an extended Tellinen hysteresis model for the 2-D hysteresis behavior $\varepsilon(B,\sigma)$ of the strain of MSM materials. Two variants of the model have been implemented as lumped network elements in Modelica.

The first variant used trial functions for an analytical approximation of the measured hysteresis envelope surfaces. The second variant interpolated these surfaces directly from a grid of experimentally measured sampling points and numerically computed their partial derivatives.

The first variant was reported to be numerically more stable and faster, whereas the second variant presents a more elegant and accurate method for capturing specific material behavior.

The models reproduce the typical arrangement of MSM materials in actuator applications having a homogeneous magnetic field perpendicular to the stroke axis, and compressive stress acting as both load and mechanical reset. The models are capable of simulating arbitrary outer and inner hysteresis trajectories. Their application was successfully demonstrated by means of a multi-domain network model using Dymola.

A dedicated testing apparatus and automated test methods for the measurement of the hysteresis envelope surfaces have been developed. These methods were employed for the characterization of a commercially available MSM sample.

A validation case with simultaneously varying magnetic flux and load revealed good agreement between measurements and simulation results for both modeling approaches. The availability of additional trial functions could improve the accuracy of future simulations as new MSM materials are made available. The models developed herein are particularly well suited for system simulation in the development and optimization process of MSM-based actuators due to their low computational expense.

A principal weakness of the Tellinen model is the limited capturing of the inner loop hysteresis behavior. To partially overcome this deficiency and increase the accuracy of inner loop behavior, the linear factors k_{B} and k_{σ} could be replaced by more sophisticated formulations. Moreover, future investigations will consider temperature and material aging effects. Finally, it is also conceivable to apply the extended Tellinen model to other solid-state actuators such as thermal shape memory actuators or other phase change materials.

ACKNOWLEDGMENT

The authors would like to thank E. Haufe and M. Kollewe for their excellent work and for their respective efforts toward the LabVIEW programming and mechanical design of the testing apparatus.

REFERENCES

[1] K. Ullakko, J. K. Huang, C. Kantner, R. C. O'Handley, and V. V. Kokorin, "Large magnetic-field-induced strains in Ni_2MnGa single crystals," *Appl. Phys. Lett.*, vol. 69, no. 13, pp. 1966–1968, Sep. 1996.

[2] V. A. Chernenko, E. Cesari, V. V. Kokorin, and I. N. Vitenko, "The development of new ferromagnetic shape memory alloys in Ni-Mn-Ga system," *Scripta Mater.*, vol. 33, no. 8, pp. 1239–1244, 1995.

[3] E. Pagounis and H. Schmidt, "Progress in developing smart magnetic materials for advanced actuator solutions," in *Proc. 13th Int. Conf. Actuat.*, Bremen, Germany, Jun. 2012.

[4] A. Hubert, N. Calchand, Y. Le Gorrec, and J.-Y. Gauthier, "Magnetic shape memory alloys as smart materials for micro-positioning devices," *Adv. Electromagn.*, vol. 1, no. 2, pp. 75–84, 2012.

[5] J. Ziske and T. Bödrich, "Magnetic hysteresis models for modelica," in *Proc. 9th Int. Model. Conf.*, München, Germany, Sep. 2012, pp. 151–158.

[6] H. Neubert, A. Kamusella, and J. Lienig, "Optimization of an electromagnetic linear actuator using a network and a finite element model," *Proc. SPIE*, vol. 7977, p. 797721, Mar. 2011.

[7] R. C. O'Handley, "Model for strain and magnetization in magnetic shape-memory alloys," *J. Appl. Phys.*, vol. 83, no. 6, pp. 3263–3270, 1998.

[8] B. Kiefer and D. Lagoudas, "Modeling the coupled strain and magnetization response of magnetic shape memory alloys under magnetomechanical loading," *J. Intell. Mater. Syst. Struct.*, vol. 20, no. 2, pp. 143–170, 2009. [Online]. Available: http://jim.sagepub.com/content/20/2/143.abstract

[9] R. N. Couch and I. Chopra, "A quasi-static model for NiMnGa magnetic shape memory alloy," *Smart Mater. Struct.*, vol. 16, no. 1, pp. S11–S21, 2007.

[10] J.-Y. Gauthier, C. Lexcellent, A. Hubert, J. Abadie, and N. Chaillet, "Modeling rearrangement process of martensite platelets in a magnetic shape memory alloy Ni_2MnGa single crystal under magnetic field and (or) stress action," *J. Intell. Mater. Syst. Struct.*, vol. 18, no. 3, pp. 289–299, 2007.

[11] L. Riccardi, G. Ciaccia, D. Naso, and H. Janocha, "Control of MSM actuators for precise positioning," in *Proc. 12th Int. Conf. New Actuat.*, Bremen, Germany, Jun. 2010.

[12] K. Schlüter and A. Raatz, "Design and control of a linear actuator driven by magnetic shape memory crystals," in *Proc. 13th Int. Conf. New Actuat.*, Bremen, Germany, Jun. 2012.

[13] A. A. Adly, I. D. Mayergoyz, and A. Bergqvist, "Preisach modeling of magnetostrictive hysteresis," *J. Appl. Phys.*, vol. 69, no. 8, pp. 5777–5779, 1991.

[14] D. Davino, A. Giustiniani, and C. Visone, "Compensation and control of two-inputs systems with hysteresis," in *Proc. J. Phys., Conf. Ser.*, vol. 268. Jan. 2011, p. 012005.

[15] D. Davino, A. Giustiniani, and C. Visone, "Design and test of a stress-dependent compensator for magnetostrictive actuators," *IEEE Trans. Magn.*, vol. 46, no. 2, pp. 646–649, Feb. 2010.

[16] E. Bindl, J. Ziske, and H. Neubert, "Short circuit tripping device based on a magnetic shape memory alloy—Principle design and model based optimization," in *Proc. 13th Int. Conf. New Actuat.*, Bremen, Germany, Jun. 2012.

[17] J. Tellinen, "A simple scalar model for magnetic hysteresis," *IEEE Trans. Magn.*, vol. 34, no. 4, pp. 2200–2206, Jul. 1998.

[18] A. A. Likhachev and K. Ullakko, "Quantitative model of large magnetostrain effect in ferromagnetic shape memory alloys," *EPJ direct*, vol. 1, no. 1, pp. 1–9, Dec. 2000.

[19] A. A. Likhachev and K. Ullakko, "Magnetic-field-controlled twin boundaries motion and giant magneto-mechanical effects in Ni–Mn–Ga shape memory alloy," *Phys. Lett. A*, vol. 275, no. 1, pp. 142–151, 2000.

[20] H. Neubert, J. Ziske, T. Bödrich, and T. Roschke, "Remarks on the application potential of magnetic shape memory alloys for miniature actuators and sensors," in *Proc. 12th Int. Conf. New Actuat.*, Bremen, Germany, Jun. 2010, pp. 758–761.

[21] M. A. Marioni, R. C. O'Handley, and S. M. Allen, "Pulsed magnetic field-induced actuation of Ni–Mn–Ga single crystals," *Appl. Phys. Lett.*, vol. 83, no. 19, pp. 3966–3968, 2003.